NURETH 14-621

STEREO PARTICLE-IMAGE-VELOCIMETRY MEASUREMENTS OF AN UNSTABLE AIR STRATIFICATION DUE TO NATURAL CONVECTION IN A MODEL CONTAINMENT

Marco Gärtner¹, Cameron Tropea¹, Suad Jakirlic¹ and Sanjeev Gupta²

¹ Institute of Fluid Mechanics and Aerodynamics / Center of Smart Interfaces

Technische Universität Darmstadt, Darmstadt, Germany

² Becker Technologies GmbH, Eschborn, Germany

Abstract

Numerical simulations of a realistic containment configuration (size of several tenths of meters) are both challenging from the physical modeling aspect and the relevant spatial/temporal resolution being necessary to capture all important mean flow and turbulence characteristics, the latter implying a correspondingly long computational time. Furthermore, full-scale experiments for model validation (CFD and lumped parameter methods; CFD -Computational Fluid Dynamics) are hardly affordable. To resolve this situation the THAIfacility (Thermal-hydraulics, Hydrogen, Aerosol and Iodine) was designed and built to enable large-scale experiments, which could then serve as a source for validation database used for the computational models improvement. This facility consists of test vessel (60 m³ volume) with a diameter of 3.4 m and a height of 9.2 m and is equipped with a broad range of measurement techniques and monitoring systems. The present study examines an unstable air stratification created by heating the lower walls and cooling the upper wall of the THAI vessel. In the center of the vessel an inner cylinder was inserted to promote establishing of a recirculating convective flow. Velocity field data were acquired using a stereo PIV system, used to cover a flow area of about 0.5m² during the stereo PIV measurements and up to 1 m² for two-velocity component (2D) measurements. Furthermore, due to the low bulk velocities involved, the system could acquire the data of the bulk motion in a quasi time resolved manner. Long averaging times of over 1000 s allowed the estimation of the turbulent flow quantities (all velocity and Reynolds-stress components). Selected time-averaged and instantaneous flow fields illustrating mean flow and turbulence structure within the containment configuration in the case of the unstable air stratification due to natural convection will be shown and appropriately discussed.

Introduction

Any nuclear accident involves extremely complex fluid mechanics phenomena. This makes the numerical simulation aiming at predicting the relevant outcomes particularly challenging. For instance, if the main cooling circuit is open the water inside the core will start to boil, and, due to the poor cooling, the temperature at the fuel rods will increase. At high temperatures the zirconium alloy, from which the rods are fabricated, begins to oxidize. Moreover, there is a

danger that the hydrogen produced in this oxidation process can be released into the containment forming an ignitable mixture. Furthermore, the geometry of the facility can be very complex, consisting of a number of sections and different chambers. Some of the major impact factors affecting the flow in a real accidental situation would be:

- Pressure driven flow (high pressure in the main cooling circuit)
- Multiphase flow (Air-steam-water-plume)
- Phase changes (at the cold concrete structures and on the steel shielding)
- Internal heat sources (radioactive progeny)

Aiming at improvement of the predictive capabilities a step-by-step approach for a benchmark experiment has been initiated, with the goal of using the obtained data for the physical models validation. These experiments take place in the THAI test facility – a large vessel with a volume of approximately 60 m³. A large reference database will be established by investigating sequentially more complex flow situations, starting with the baseline case (flow forced by a blower), then proceeding to the pressure-driven flows, natural convection and helium transport, as well as the steam plume flows and configurations involving phase changes. The current experimental series (denoted by TH 21 and TH 22; in some references these configurations are denoted as CV3 and CV4 respectively) addressed natural convection and helium transport. To create an unstable stratification the lower walls of the container were heated and the upper wall was cooled. In the TH 22 case, the thermal stratification was additionally augmented with a helium gas cloud. The thermal boundary conditions of the two experiments were the same. During the experiments various measurements were carried out ([1], [2]):

- Temperature measurements: using thermocouples
- Flow field: vane wheel anemometers, Laser Doppler Velocimetry LDV, Particle Image Velocimetry PIV (including stereo PIV)
- Helium concentration: multichannel mass spectrometer (TH 22) and conductivity sensors (TH 21)

The helium transport results from the TH 22 experiment will not be discussed in the present paper.

1. Experimental setup

A schematic of the experimental facility is given in Figure 1, where an inner cylinder is shown, which forces the bulk flow recirculation. All experiments followed the same procedure. First the vessel was sealed with the closure lid. Then the heating and cooling of the outer walls were initiated. After a certain time the temperatures of the heating jackets, the cooling jacket and the

air reached their constant values – the experiments were performed in this steady-state phase. The corresponding operating conditions are given in Table 1.

Table 1 – Operating conditions for the steady state case

D = 3.2 m
$H_c = 1,500 \text{ m}$
$H_h = 4,750 \text{ m}$
H = 9,200 m
$T_{c} = 313 \text{ K}$
$T_h = 393 \text{ K}$
$T_{\infty} = 363 \text{ K}$
P = 1,20 bar
$t_s > 14.400 \text{ s}$
$Ra = 1,31 * 10^{11}$
$Gr = 1,86 * 10^{11}$
$Nu_c = 226$
$Nu_h = 573$

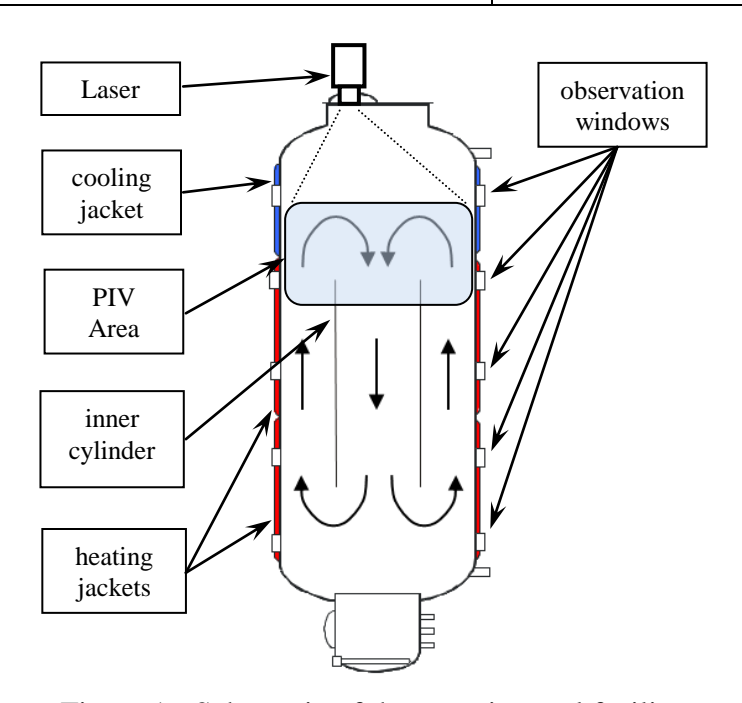


Figure 1 - Schematic of the experimental facility

2. Particle image velocimeter

Optical access into the vessel was limited to certain observation windows as shown in Figure 1. The laser was mounted on top of the vessel (Figure 1). A horizontal cross-section of the vessel is shown in Figure 2, where the positions of the light sheets for the different measurement planes can be seen.

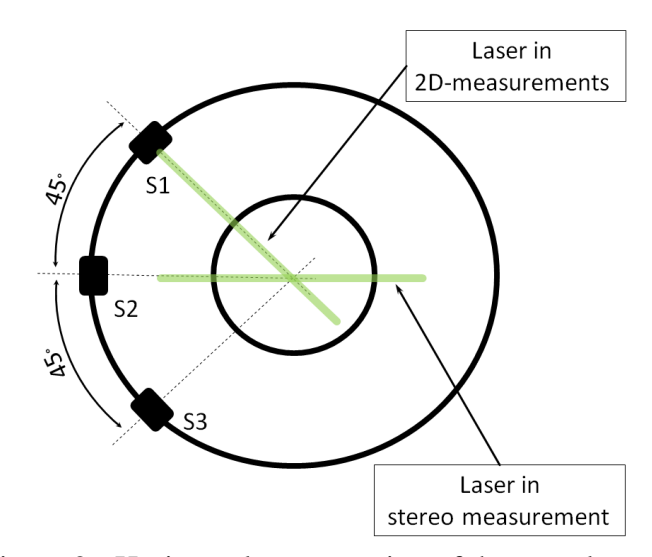


Figure 2 - Horizontal cross-section of the vessel

During the TH 21 experiments the window S2 was used for the 2D measurement and the windows S1 and S3 for the stereo measurement. In the TH 22 cases the window S2 was used. The positions of the measurement windows within the laser light sheet for the different experiments are shown in Figure 3. For clarity the windows have been projected onto a common plane.

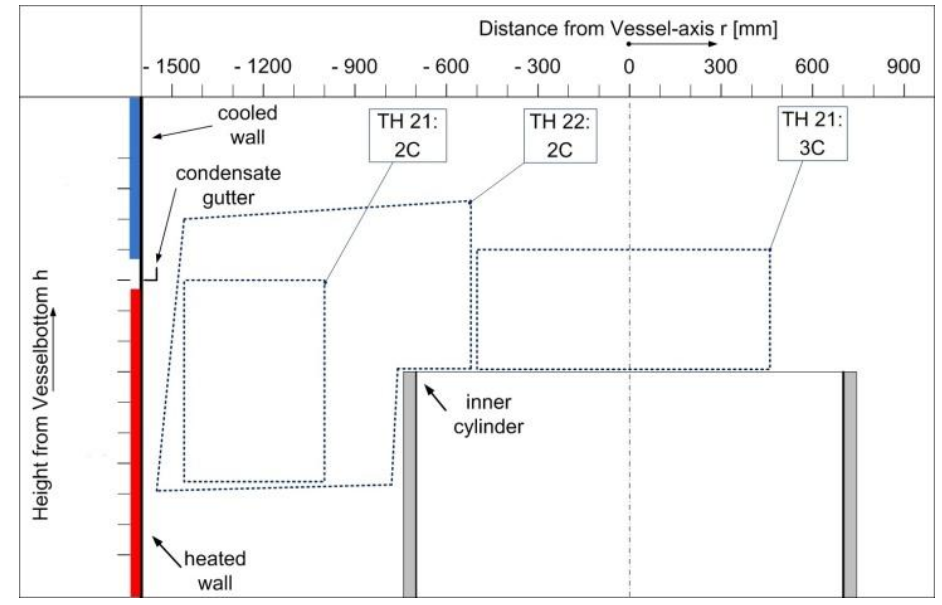


Figure 3 - Position of the different measurement windows (2C/3C stays for two/three components)

An overview of the measurement duration of individual experiments is given in Table 2. In the TH 22 experimental series all PIV-measurements were performed before the Helium was introduced.

T 11 0		. 1
Table 7	Hyperimen	tal matriv
1 aut 2	Experimen	tai iiiatiin

Experiment	Frequency	Measurement time(s)
TH 21		
2D	1 Hz	1500 s
Stereo	1 Hz	1000 s
	5 Hz	200 s
TH 22		
2 D	1 Hz	1000 / 1500 / 1600 s
	5 Hz	200 / 300 / 400 s

Calibration for the stereo measurement is complicated because it is not possible to use a single target mounted in the vessel. It is also not possible to move the target for different calibration positions z. Hence the Tsai procedure was used. With this calibration model it is not necessary to move the target during calibration [4]. As a target a sheet of paper mounted in a frame was used. This target was adjusted inside the light sheet until the laser light "walked" through the paper. The scheme and the actual construction of the target with crosshair markers are shown in Figure 4.

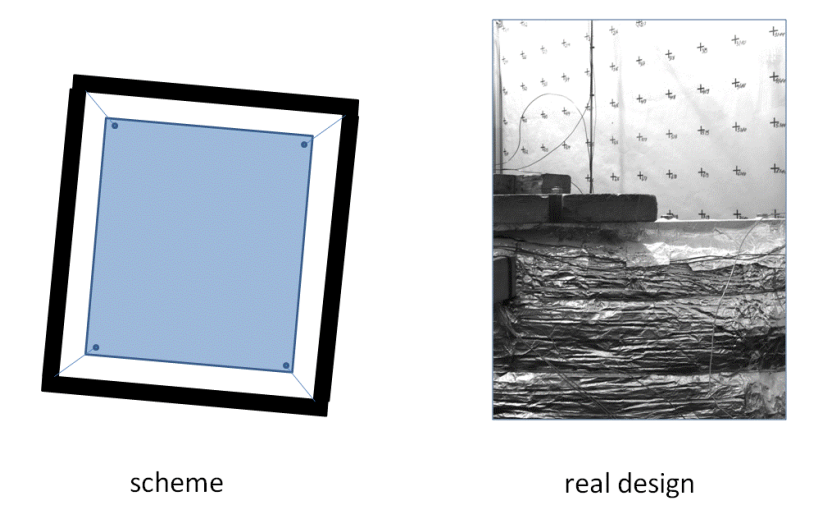


Figure 4 - Stereo target

The specification of the PIV instrumentation is given in Table 3.

Table 3 –PIV specifications

Camera		
Type	PCO Pixelfly QE	
Resolution	1392 x 1024 pixel	
Dynamic range	12 bit	
Frame rate	12 fps (full frame)	
Scheimpflug angle	φ ≈ 1°	
(for stereo only)	$\psi \sim 1$	
Lens		
Type	Canon Ultrasonic EF II USM	
Focal length	f = 14 mm	
f-number	f# = 2,8	
Laser		
Type	New Wave ND:YAG	
Pulse energy	E = 120 mJ	
Pulse distance	$\Delta t = 4 \text{ ms}$	
Light sheet thickness	$a \approx 5 \text{ mm}$	
Seeding		
Type	Expancel® DET 100	
Density	$\rho = 25 + /-3 \text{ kg/m}^3$	
Diameter range	$d_p = 80 100 \mu m$	

3. Post processing

The goal in the post processing was to obtain as many valid vectors as possible; hence conservative processing algorithms were used. After an adaptive cross-correlation with an interrogation area size of 64 x 64 pixels and a 50 % overlap a window velocity filter and a local median filter based on the standard deviation were used. Afterwards an interpolation of the filtered vectors was performed. The rate of valid vectors was of the order of 99 %. From the velocity vectors the following quantities (third velocity component is present only in the stereo PIV measurements) were then estimated as follows, [3]:

• Velocities
$$u_i = f(x, y, t)$$
 (1)

The 14th International Topical Meeting on Nuclear Reactor Thermalhydraulics, NURETH-14 Toronto, Ontario, Canada, September 25-30, 2011

• Shear strain rate:
$$\mathcal{E}_{xy} = \left(\frac{\partial v}{\partial x} + \frac{\partial u}{\partial y}\right) \tag{2}$$

• Normal strain rate x:
$$\varepsilon_{xx} = \frac{\partial u}{\partial x}$$
 (3)

• Normal strain rate y:
$$\varepsilon_{yy} = \frac{\partial v}{\partial y}$$
 (4)

• Vorticity z:
$$\omega_z = \left(\frac{\partial v}{\partial x} - \frac{\partial u}{\partial y}\right) \tag{5}$$

The assumption of an incompressible flow regime $(\nabla \cdot \vec{u} = 0)$ leads to the third normal strain component:

• Normal strain rate z:
$$\varepsilon_{zz} = \frac{\partial w}{\partial z} = \left(-\frac{\partial u}{\partial x} - \frac{\partial v}{\partial y} \right)$$
 (6)

Using a time averaging and a decomposition of the velocity into a mean part and a fluctuating part yields:

$$\overline{\hat{U}_i \hat{U}_j} = U_i U_j + \overline{u'_i u'_j} \tag{7}$$

The first and the second part of the equation are known, hence the third part can be solved. With this it is possible to calculate the turbulent kinetic energy:

$$k = \frac{1}{2} \left(\overline{u'u'} + \overline{v'v'} + \overline{w'w'} \right) \tag{8}$$

In a 2D measurement, where only two velocity components can be measured, the fluctuating part of the third component can be estimated. Using the assumption of the isotropic turbulence $(\overline{w'w'} = 2k/3)$ the kinetic energy of turbulence is accordingly:

$$k = \frac{3}{4} \left(\overline{u'u'} + \overline{v'v'} \right) \tag{9}$$

With stereo PIV the full Reynolds stress tensor in the measurement plane can be determined:

$$T_{ij} = -\rho \cdot \overline{u_i' u_j'} \tag{10}$$

In general time-resolved PIV measurements require high laser repetition rates and high camera frame rates, depending on the integral time scales of the flow. The integral time scale I_x can be estimated using a characteristic length scale L_c and a characteristic velocity scale u_c :

$$I_x \approx \frac{L_c}{u_c} \tag{11}$$

Using the diameter of the vessel (d = 3.2 m) as characteristic length and 0.5 m/s as characteristic velocity yields the integral time scale of 6.4 s for this experimental series.

For time-resolved measurements, the number of measurements must be increased beyond two samples per one I_x (statistical independence). The number of measurements n per integral time scale is given as:

$$n = 2fL_c u^{-1} \tag{12}$$

Using 5 Hz as the maximum frequency of the measurement system and the diameter of the vessel as the characteristic length scale, the number of measurements per integral time scale is given in Figure 5 for various characteristic velocities. In this study, typical velocities were 0.5 m/s, yielding a large value of n and an effective time resolved measurement for the bulk motion.

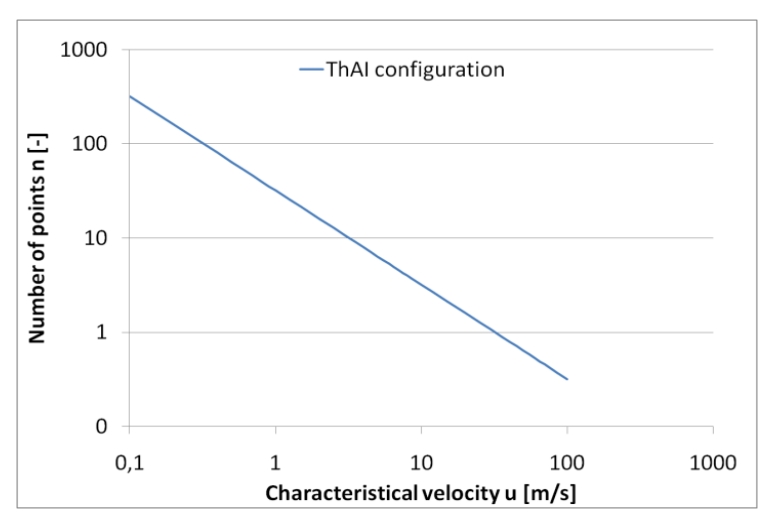


Figure 5 - Number of PIV measurements per integral time scale in the THAI facility

4. Measurement results

Due to the very large amount of data which was collected only a representative sample of measurements will be shown and discussed. However, the main conclusions remain unaltered. First, the (time-averaged) mean values of each arrangement will be shown, followed by a discussion of the time dependent results. Finally the Reynolds stress components will be presented.

4.1 Mean values

The mean values of the flow in the steady state phase of the experiment are of great importance with respect to the direct comparison with complementary numerical simulations (which are in

progress). In Figure 6 the results for the TH 21 2D PIV experiments are shown. The buoyancy effects originating from the temperature gradient between the heated wall and the surrounding air cause an upward flow characterized by a wall-jet-like boundary layer of an appropriate thickness. In the upper part of the containment a downward flow along the cold walls was created. These two streams collide at a position corresponding to the location of the condensate gutter forming a horizontal layer, actually a barrier separating two sub-regions, flowing radially towards the containment vertical axis. One can see the strong curvature of the flow at the dividing line between the cold and the hot air. As a consequence a recirculation between the heated wall and the inner cylinder is established. The flow velocities are of a comparable low intensity.

In Figure 7 the same region is displayed during the TH 22 experiments. Important improvements were achieved to reduce the reflections on the camera images and to extend the measurement area. Hence it was possible to measure the flow closer to the wall. The bulk flow exhibits similar behavior as in the TH 21 experiments, but important details could be captured. One can see the maximum velocity within the wall-boundary layer (red area) reducing towards a value close to zero corresponding to the position representing the center of the recirculating region. Also visible is the region of the colliding hot and cold streams resembling a stagnation region (blue area in the upper left corner at the condensate gutter). Afterwards the flow is strongly curved towards the vessel center exhibiting locally a certain acceleration (transition from the blue to the red area in the region of the dividing layer). After that flow intensity in the horizontal layer relaxes until the central part was reached. Here the flow is curved towards the negative vertical direction. This action is followed by a certain acceleration (see red area in Figure 8). Along the inner cylinder walls and the containment axis the flow develops downwards. As the final consequence of the thermal stratification the counter rotating loops were created.

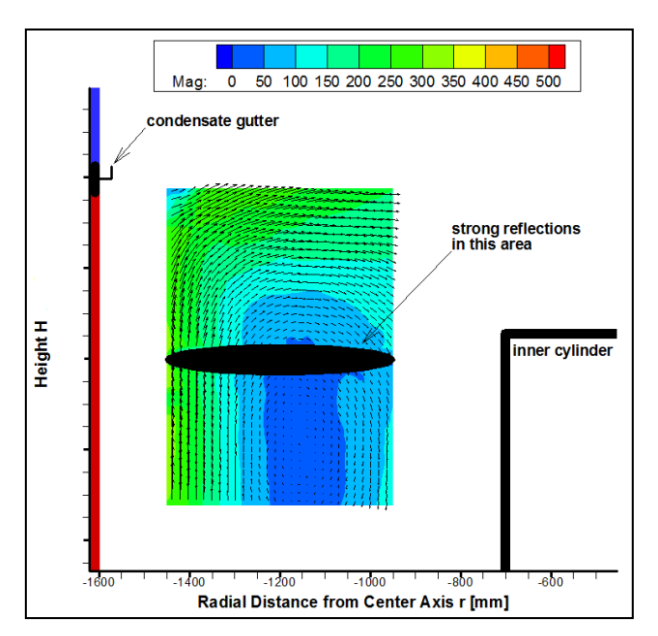


Figure 6 - Velocity vector plots and the mean velocity contours colored by the velocity magnitude (TH 21 case)

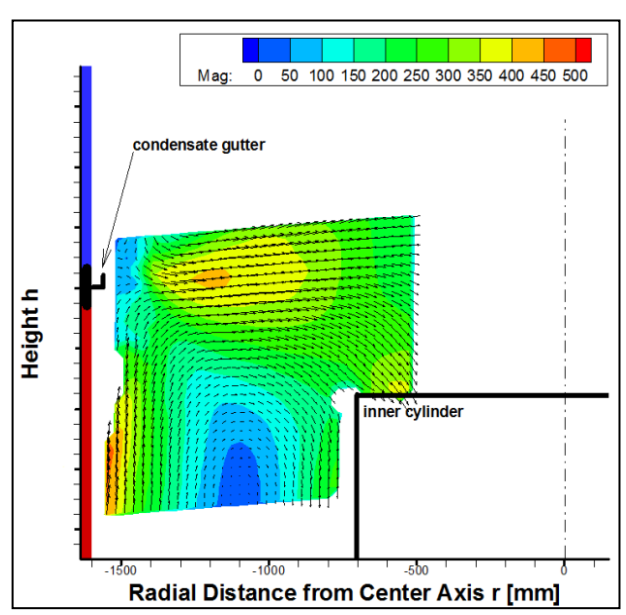
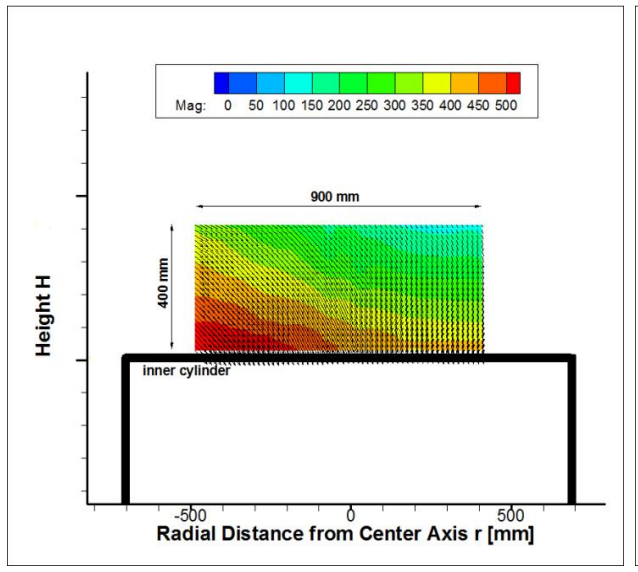


Figure 7 - Velocity vector plots and the mean velocity contours colored by the velocity magnitude (TH 22 case)

In Figure 8 and Figure 9 the results of the stereo measurements are shown. The mean value of the out-of-plane velocity component w is small compared to the mean values of the in-plane components u and v. But this does not mean that this w component is negligible. This will be illustrated in the next section, where the temporal behavior of the flow will be examined. The instantaneous velocity values are substantially higher indicating a strong flow unsteadiness in the circumferential direction. This is especially the case in the region of the strongest curvature where higher frequency oscillations were induced. Generation of a bulk swirling flow of a lower intensity at this location is possible.



W: -500 -400 -300 -200 -100 0 100 200 300 400 500

900 mm

Inner cylinder

Radial Distance from Center Axis r [mm]

Figure 8 - Magnitude of the mean velocity measured by the stereo PIV method (TH 21 case)

Figure 9 - Magnitude of the out-of-plane velocity component measured by the stereo PIV method (TH 21 case)

In Figure 10 the profiles of the vertical velocity component v at different elevations inside the vessel during the TH 21 and TH 22 experiments are shown. One notes the velocity maximum being situated within the wall layer and a steep velocity gradient relaxing to (almost) a zero value arising from the flattened velocity profile (characterized by negative velocity values) corresponding to the vessel center. Mutual agreement between the data extracted at the same vertical positions within the annulus (left part of the diagram) is very good. The data of the TH 21 experiment (blue line) fit well with TH 22 results (red line). Also, the matching of the stereo measurements from the TH 21 experiment with the 2D measurements from the TH 22 case is reasonable (central part of the diagram). The small offset might be caused by the difference in the elapsed time from the start of the experiment for the single measurements. In addition to that the light sheet of the stereo measurements was rotated by 45° to the 2D experiments, which led to slightly different results. The matching of the horizontal velocity component u is not that good (not shown here). Let us recall that the bulk flow within the containment occurs mostly in the vertical direction. It implies, that the v-impulse represents the governing part (cause of the buoyancy) of the flow and is therefore much more stable, than the u-part.

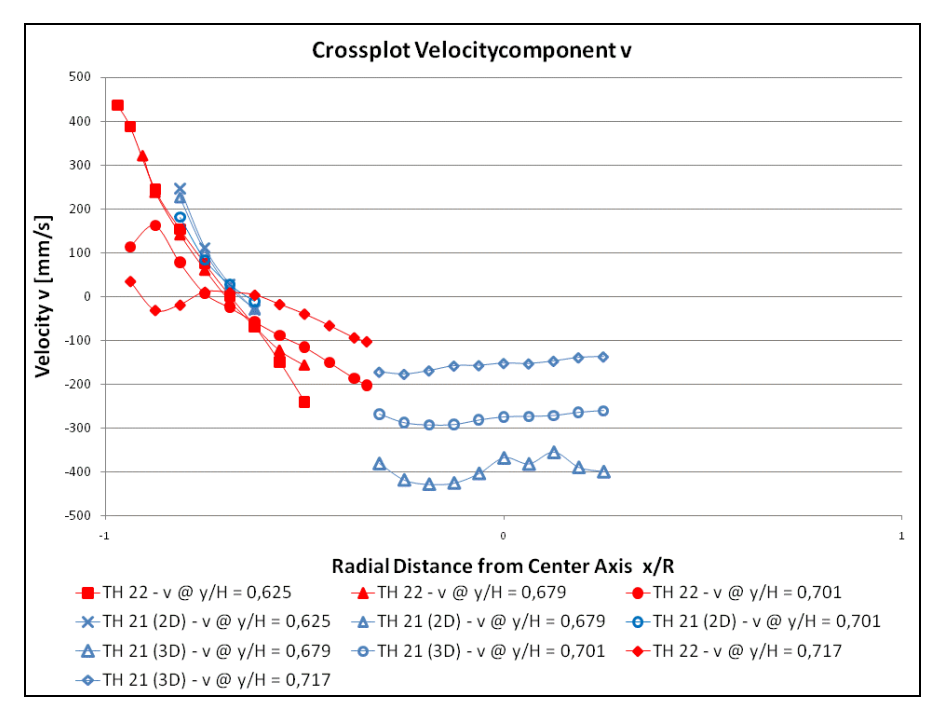


Figure 10 - Profiles of the velocity component v at different levels corresponding to the TH 21 and TH 22 experiments

In Figure 11 the development of the out-of-plane component w over a short period of time is depicted. One can observe fairly intensive turbulence activity in this area (the position of the measurement window - denoted by 3C - is shown in Figure 3). As discussed previously the mean value of w is quite small but the instantaneous value is of the same order of magnitude as the other two fluctuating velocity components. The position of its maximum coincides with the position of the strongest curvature. It is plausible to presume that here some secondary shearing pertinent to a swirl of a certain intensity occurs.

Figure 12 displays the instantaneous velocity fields of the TH 22 experiment at several time instants. The position of the measurement window is that shown in Figure 7. The results obtained revealing a recirculation loop between the containment walls and the inner cylinder walls follow the pattern typical for this configuration. One can also note a strong time dependence. An intensive temporal change of the velocity maximum (yellow/red area) is obvious.

In Fig.13 the instantaneous fields of the kinetic energy of turbulence k over a certain period of time is shown. These results represent only a very short snap-shot of the whole measurement campaign. Despite of that some important observations with respect to the general flow and turbulence behavior could be obtained. The maximum of the turbulent kinetic energy (red area) is situated in the region exhibiting strongest mean flow deformation. In addition to the mean flow straining (steep velocity gradients), representing the most important source of turbulence generation, the turbulence production originates also from the streamline curvature whose intensity is temporally dependent (according to the discussion related to Figure 12). Furthermore, the turbulence production is strongly promoted by flow and turbulence unsteadiness.

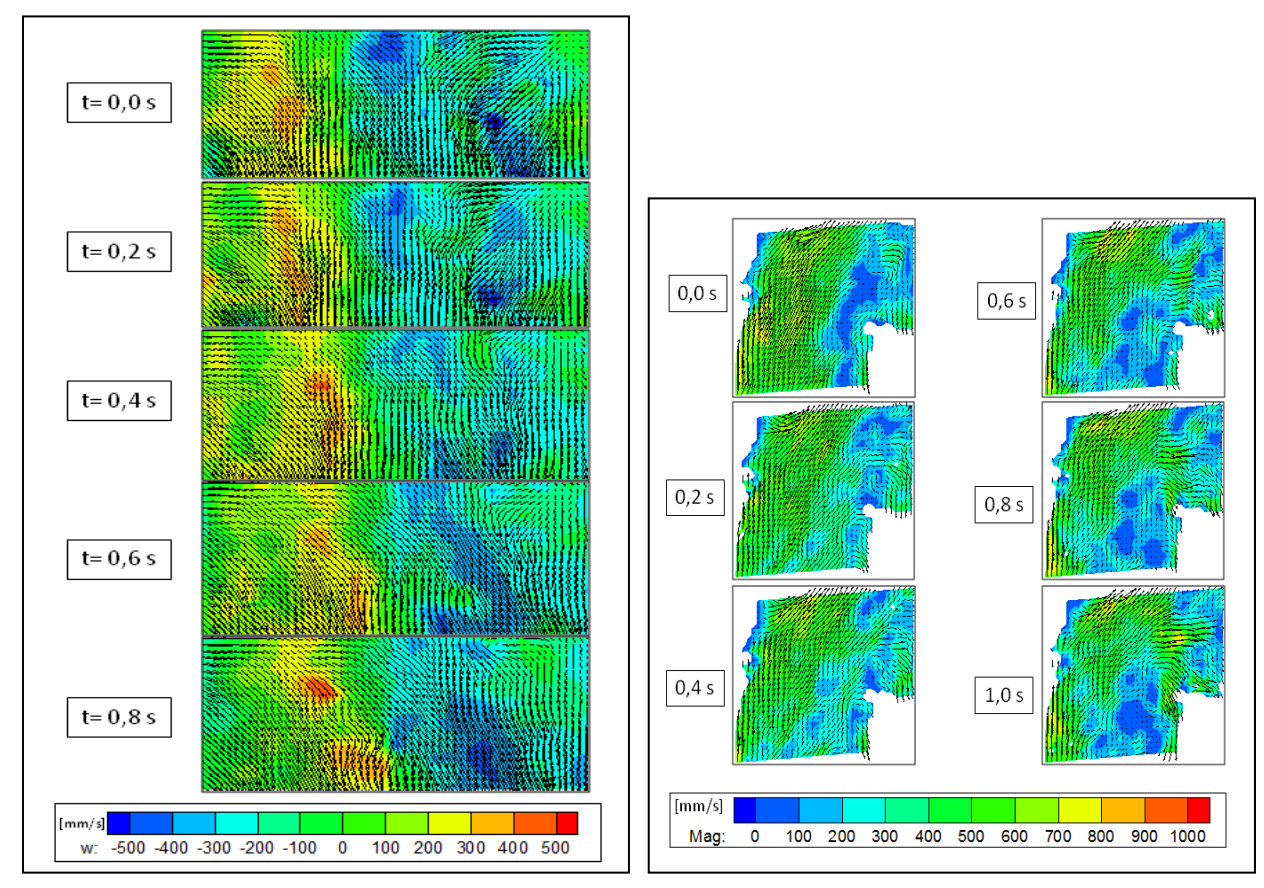


Figure 11 - Mean velocity magnitude in the TH 22 experiment (instantaneous)

Figure 12 - Mean velocity magnitude in the TH 22 experiment (instantaneous)

The comparison of the instantaneous fields (a snap-shot at one time instant) of individual Reynolds stress components is displayed in Figure 14. Some insight into the flow physics can be extracted from these images. The out-of-plane Reynolds stress component is much larger than the other two, contributing mostly to the kinetic energy of turbulence. Similar situation is pertinent to a swirling flow configuration where the circumferential components are the largest one, the fact being especially visible in the flow core. It could be regarded as an indication for a locally induced swirling motion. Furthermore, the measurements reveal a somewhat higher intensity of the normal (vertical) Reynolds stress component compared to the horizontal one. The latter outcome was expected keeping in mind that the most intensive mean flow occurs in the vertical direction.

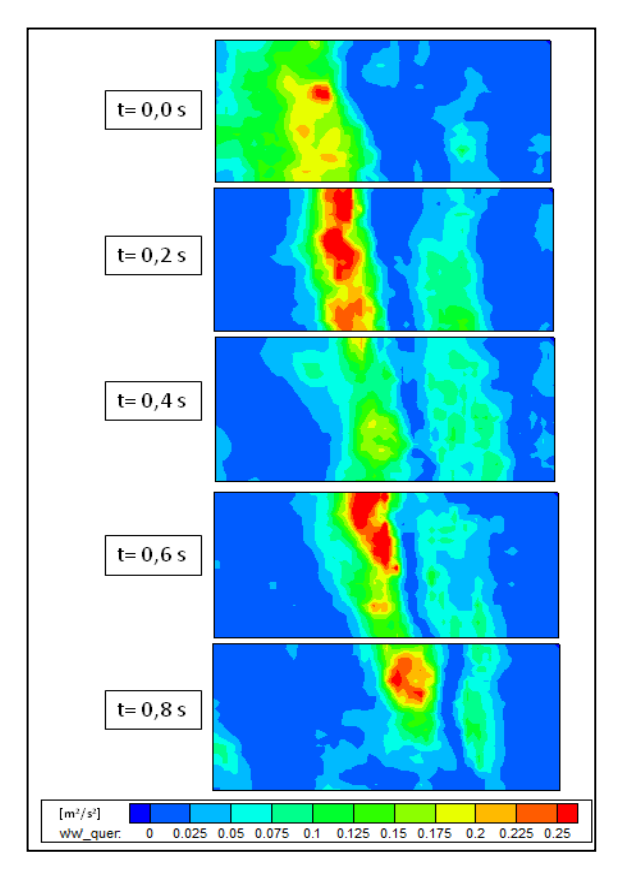


Figure 13 - Temporal behavior of the turbulent kinetic energy in the TH 21 experiment (instantaneous)

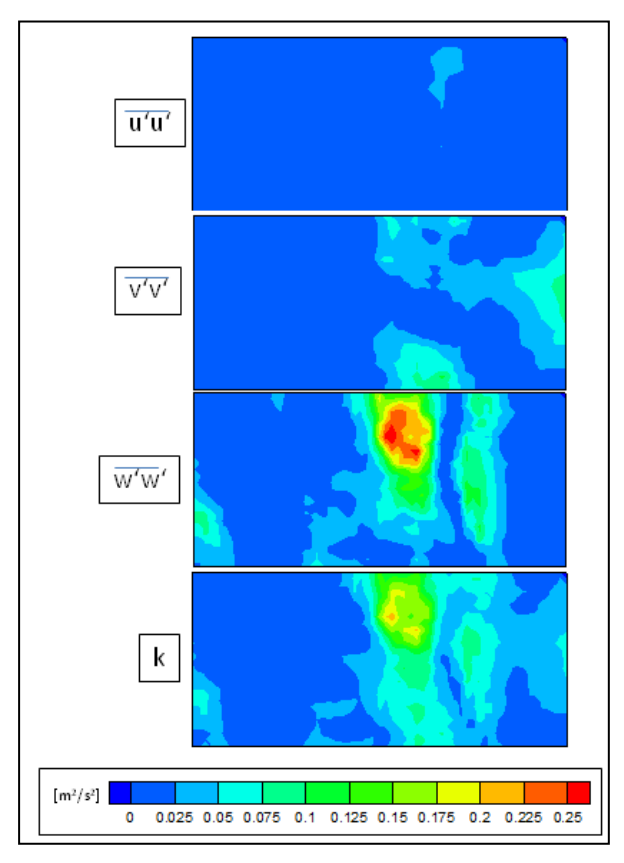


Figure 14 - Reynolds stress components and kinetic energy of turbulence TH 21 (instantaneous)

5. Conclusion

An experimental database has been generated serving for the CFD models validation applicable to large-scale flows typical of nuclear containment situations. This database contains not only mean values, but also fluctuating components. The results of the two experimental series are comparable with each other, both being conducted under similar boundary conditions. But it is necessary to note, that the TH 22 series was about the dissipation of a light gas cloud providing much more detailed information than it has been presented presently.

The observed flow area is large – the stereo measurement window is approximately 400 x 900 mm. Also the measurements are quasi time resolved for the bulk motion. A tracking of the flow over time is possible. It is important to note that the out-of-plane fluctuations are fairly intensive, even if the mean value of this velocity component is comparatively small. A two-dimensional simulation (CFD) of this flow is therefore inappropriate, because the important effects corresponding to the strong unsteadiness in the circumferential direction will not be captured.

6. Acknowledgements

The financial support of the German Federal Ministry of Economics and Technology (BMWi) is gratefully acknowledged.

7. References

- [1] K. Fischer, S. Gupta, A. Kühnel: Technischer Fachbericht ThAI Konvektionsversuch TH 21; Becker Technologies GmbH; Eschborn; 2009
- [2] K. Fischer, S. Gupta, B. Balewski, A. Kühnel: Technischer Fachbericht ThAI Versuch TH 22: Auflösung einer Leichtgasschicht durch Naturkonvektion; Becker Technologies GmbH; Eschborn; 2010
- J. Kompenhans, M. Raffel, C. Willert, S. Wereley: **Particle Image Velocimetry A practical Guide**; 2. Auflage; Springer; Berlin; 2007;
- [4] S. Soloff, R. Adrian, Z. Liu: Distortion compensation for generalized stereoscopic particle image velocimetry; Measurement Science and Technology 8:1441 1454, 1997
- [5] C. Tropea, A. Yarin, J. Foss: **Springer Handbook of Experimental Fluid Mechanics**; Springer; Heidelberg; 2007;